Experimental Application of Extremum Seeking on an Axial-Flow Compressor

Hsin-Hsiung Wang, Simon Yeung, and Miroslav Krstić, *Senior Member, IEEE*

***Abstract*—We show an application of the method of extremum seeking to the problem of maximizing the pressure rise in an axial flow compressor. First we apply extremum seeking to the Moore–Greitzer model and design a feedback scheme actuated through a bleed valve which simultaneously stabilizes rotating stall and surge and steers the system towards the equilibrium with maximal pressure. Then we implement the scheme on a compressor rig in Murray's laboratory at the California Institute of Technology. We perform stabilization of rotating stall via air injection and implement extremum seeking through a slow bleed valve. The experiment demonstrates that extremum seeking ensures the maximization of the pressure rise starting on either side of the stall inception point. The experiment also resolves a concern that extremum seeking requires the use of periodic probing—the amplitude of probing needed to achieve convergence is far below the noise level of the compressor system (even outside rotating stall).**

***Index Terms*—Aeroengine compressors, air injection, bleed valve, extremum seeking, rotating stall, surge.**

I. Introduction

EVEN though the methods of "extremum seeking" [1], [6], [7], [9], [12], [13], [17], [21], [22], [24], [26] have been in existence since the 1950's, much before the theoretical breakthroughs in adaptive linear control of the 1980's, a rigorous proof of stability did not exist before the recent paper [16]. We employed the tools of averaging and singular perturbations to show that solutions of the closed-loop system converge to a small neighborhood of the extremum of the equilibrium map (the size of the neighborhood is proportional to the adaptation gain and the amplitude and the frequency of a periodic signal used to achieve extremum seeking) and highlight a fundamentally nonlinear mechanism of stabilization in an extremum seeking loop. We briefly summarize the results from [16] in Section II.

Our main objective in the present paper is to apply the extremum seeking scheme to an axial-flow compressor to maximize its pressure rise. The idea to use extremum control for maximizing the pressure rise in an aeroengine compressor is not new. As far back as in 1957, G. Vasu of the NACA (now NASA) Lewis Laboratory published his experiments in which he varied the fuel flow to achieve maximum pressure [27]. While his engine was apparently not of the kind that could enter either rotating stall or surge instabilities (so local stabilizing feedback was not necessary), it is remarkable that he recognized the opportunity to maximize the pressure by extremum seeking feedback long before the compressor models of the 1970's and 1980's have emerged and the dynamics of compression systems have been understood.

In Section III we first present an application of extremum seeking to a compressor model with bleed valve actuation. We achieve maximization of the compressor pressure rise in the presence of an uncertain "compressor characteristic" whose argument of the maximum is unknown. Our extremum seeking scheme benefits from our recent results on stabilization of stalled equilibria in "deep-hysteresis" compressors [28]. In Section III-C we give a brief simulation case study which shows that major improvements in the compressor efficiency are potentially achievable using the extremum seeking scheme. At the same time, actuation (and sensing) requirements are much less demanding than those for stabilization of stalled equilibria.

The main results of the paper are experimental and they are shown in Section IV where we implement extremum seeking on an axial-flow compressor in Murray's laboratory at the California Institute of Technology. The extremum seeking is implemented via a slow bleed valve, while rotating stall stabilization is performed with air injection, as in [4]. The results demonstrate the effectiveness of extremum seeking in maintaining maximal pressure rise while preventing rotating stall (of either large or small amplitude).

II. Extremum Seeking Scheme

In [16] we described a control scheme which can enforce convergence to the peak of an output equilibrium map. Consider a general single input–single output (SISO) nonlinear model

$$\dot{x} = f(x,u) \tag{2.1}$$

$$y = h(x) \tag{2.2}$$

where $x \in \mathbb{R}^n$ is the state, $u \in \mathbb{R}$ is the input, $y \in \mathbb{R}$ is the output, and $f : \mathbb{R}^n \times \mathbb{R} \to \mathbb{R}^n$ and $h : \mathbb{R}^n \to \mathbb{R}$ are smooth.

Manuscript received March 5, 1998; revised December 14, 1998. Recommended by Associate Editor, F. Ghorbel. The work of H.-H. Wang and M. Krstić was supported in part by the Air Force Office of Scientific Research under Grant F49620-96-1-0223 and in part by the National Science Foundation under Grant ECS-9624386. The work of H.-H. Wang and S. Yeung was supported in part by the Air Force Office of Scientific Research under Grant F49620-95-1-0409.

H.-H. Wang is with the Department of Electrical Engineering, Oriental Institute of Technology, Panchiao, Taipei 220, Taiwan (e-mail: swang@www.ee.oit.edu.tw).

S. Yeung is with General Electric Company, Schenectady, NY 12301 USA (e-mail: yeung@cdr.ge.com).

M. Krstić is with the Department of Mechanical and Aerospace Engineering, University of California, San Diego, La Jolla, CA 92093-0411 USA (e-mail: mkrstic@ames.ucsd.edu).

Publisher Item Identifier S 1063-6536(00)01785-1.

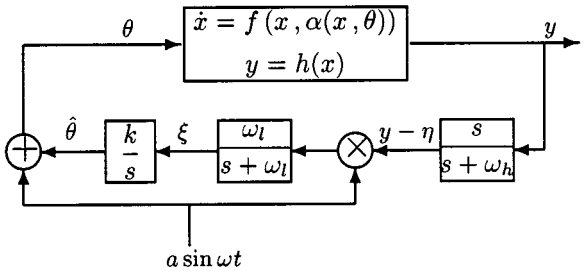

Fig. 1. A peak seeking feedback scheme.

Suppose that we know a smooth control law $u = \alpha(x, \theta)$ parameterized by a scalar parameter θ.

Assumption 2.1: There exists a smooth function $l : \mathbb{R} \to \mathbb{R}^n$ such that

$$f(x, \alpha(x, \theta)) = 0 \quad \text{if and only if } x = l(\theta). \tag{2.3}$$

Assumption 2.2: For each $\theta \in \mathbb{R}$, the equilibrium $x = l(\theta)$ of the closed-loop system is locally exponentially stable.

Assumption 2.3: There exists $\theta^* \in \mathbb{R}$ such that

$$(h \circ l)'(\theta^*) = 0 \tag{2.4}$$

$$(h \circ l)''(\theta^*) < 0. \tag{2.5}$$

Thus, we assume that the output equilibrium map $y = h(l(\theta))$ has a *maximum* at $\theta = \theta^*$. Our objective is to develop a feedback mechanism which maximizes the steady-state value of y but without requiring the knowledge of either θ^* or the functions h and l. Our feedback scheme is shown in Fig. 1. It is an extension of a simple method for seeking extrema of *static* nonlinear maps [6].

The basic idea of operation of the peak seeking scheme is as follows. The scheme employs a *slow* periodic perturbation $a \sin \omega t$ which is added to the signal $\hat{\theta}$, our best estimate of θ^*. If the perturbation is slow, then the plant appears as a static map $y = h \circ l(\theta)$ and its dynamics do not interfere with the peak seeking scheme. If $\hat{\theta}$ is on either side of θ^*, the perturbation $a \sin \omega t$ will create a periodic response of y which is either in phase or out of phase with $a \sin \omega t$. The high-pass filter $s/(s + \omega_h)$ eliminates the "dc component" of y. Thus, $a \sin \omega t$ and $(s/(s+\omega_h))y$ will be (approximately) two sinusoids which are

- in phase for $\hat{\theta} < \theta^*$
- out of phase for $\hat{\theta} > \theta^*$.

In either case, the product of the two sinusoids will have a "dc component" which is extracted by the low-pass filter $\omega_l/(s + \omega_l)$. The dc component ξ can be argued to be approximately the sensitivity $(a^2/2)(h \circ l)'(\hat{\theta})$. Then the integrator $\dot{\hat{\theta}} = (k/s)\xi$ is approximately the gradient update law $\dot{\hat{\theta}} = k(a^2/2)(h \circ l)'(\hat{\theta})$ driven by the sensitivity function, which tunes $\hat{\theta}$ to θ^*.

The parameters in Fig. 1 are selected as

$$\omega_h = \omega \omega_H = \omega \delta \omega'_H = O(\omega \delta) \tag{2.6}$$

$$\omega_l = \omega \omega_L = \omega \delta \omega'_L = O(\omega \delta) \tag{2.7}$$

$$k = \omega K = \omega \delta K' = O(\omega \delta) \tag{2.8}$$

where ω and δ are small positive constants and ω'_H, ω'_L, and K' are $O(1)$ positive constants. a also needs to be small. From (2.6) and (2.7) we see that the cutoff frequencies of the filters need to be lower than the frequency of the perturbation signal. In addition, the adaptation gain k needs to be small. Thus, the overall feedback system has three time scales:

- fastest—the plant with the stabilizing controller;
- medium—the periodic perturbation;
- slow—the filters in the peak seeking scheme.

Theorem 2.1 ([16]): Consider the feedback system in Fig. 1 under Assumptions 2.1–2.3. There exists a ball of initial conditions around the point $(x, \hat{\theta}, \xi, \eta) = (l(\theta^*), \theta^*, 0, h \circ l(\theta^*))$ and constants $\bar{\omega}, \bar{\delta}$, and $\bar{a}$ such that for all $\omega \in (0, \bar{\omega}), \delta \in (0, \bar{\delta})$, and $a \in (0, \bar{a})$, the solution $(x(t), \hat{\theta}(t), \xi(t), \eta(t))$ exponentially converges to an $O(\omega + \delta + a)$-neighborhood of that point. Furthermore, $y(t)$ converges to an $O(\omega + \delta + a)$-neighborhood of $h \circ l(\theta^*)$.

III. Application to a Compressor Model

We now apply the peak seeking scheme of Section II to the Moore–Greitzer compressor model [20]

$$\dot{R} = \frac{\sigma}{3\pi} \sqrt{R} \int_0^{2\pi} \Psi_C(\Phi + 2\sqrt{R} \sin \lambda) \sin \lambda \, d\lambda \tag{3.1}$$

$$\dot{\Phi} = -\Psi + \frac{1}{2\pi} \int_0^{2\pi} \Psi_C(\Phi + 2\sqrt{R} \sin \lambda) \, d\lambda \tag{3.2}$$

$$\dot{\Psi} = \frac{1}{\beta^2}(\Phi - \Phi_T) \tag{3.3}$$

where the quantities are defined in Table I, and the initial condition of the state $R = A^2/4$ is physically restricted to be nonnegative, $R(0) \geq 0$. The throttle flow Φ_T is related to the pressure rise Ψ through the throttle characteristic

$$\Psi = \frac{1}{\gamma^2}(1 + \Phi_{C0} + \Phi_T)^2 \tag{3.4}$$

where γ is the throttle opening. For smaller values of γ, a compressor undergoes two instabilities, rotating stall and surge. The possibility of a debilitating effect that these two instabilities pose limits the operating envelope of today's aeroengines. A comprehensive dynamical system study in [19] showed that the Moore–Greitzer model correctly (qualitatively) predicts both of the two instabilities. Starting with [18], several control designs have emerged which apply feedback by varying the throttle opening γ to stabilize stall and surge (see [15], [28] and the references therein).

TABLE I
NOTATION IN THE MOORE–GREITZER MODEL

$\Phi = \hat{\Phi}/W - 1 - \Phi_{C0}$	$\hat{\Phi}$—annulus-averaged flow coefficient W—compressor characteristic semi-width
$\Psi = \hat{\Psi}/H$	$\hat{\Psi}$—plenum pressure rise H—compressor characteristic semi-height
$A = \hat{A}/W$	$\hat{A}$ — rotating stall amplitude
Φ_T	mass flow through the throttle/$W - 1$
θ	angular (circumferential) position
$\beta = \frac{2H}{W}B$	B — Greitzer stability parameter
$\sigma = \frac{3l_c}{m+\mu}$	l_c—effective length of inlet duct normalized by compressor radius m—Moore expansion parameter μ—compressor inertia with in blade passage
$t = \frac{H}{Wl_c}\hat{t}$	$\hat{t}$—(actual time) × (rotor angular velocity)

A. Pressure Peak Seeking for the Surge Model

For clarity of presentation, we first consider the model (3.1)–(3.3) restricted to the invariant manifold $R = 0$

$$\dot{\Phi} = -\Psi + \Psi_C(\Phi) \tag{3.5}$$

$$\dot{\Psi} = \frac{1}{\beta^2}(\Phi - \Phi_T). \tag{3.6}$$

This model is, in fact, the surge model introduced by Greitzer [10], which describes limit cycle dynamics in centrifugal compressors. The function $\Psi_C(\Phi)$ represents the "compressor characteristic," whose typical S-shape is given in Fig. 2. Our objective is to converge to the peak of this characteristic and operate the compressor with maximum pressure. Thus, we denote $x = (\Phi, \Psi)$ and $y = \Psi$. In [14] we showed that a control law of the form

$$\gamma = \frac{\Gamma + \bar{\beta}^2(c_\Psi \Psi - c_\Phi \Phi)}{\sqrt{\Psi}} \tag{3.7}$$

stabilizes equilibria parameterized by Γ. If the design parameters are chosen to satisfy $\bar{\beta}^2 > \beta, c_\Psi > 0, c_* = c_\Phi + (1/\bar{\beta}^2) > 0$, and

$$\frac{c_*}{c_\Psi} > \max_{\Phi} \frac{d\Psi_C(\Phi)}{d\Phi} \tag{3.8}$$

(which is finite), then the control law (3.7) achieves *global exponential stability* of equilibria parameterized by Γ.

In order to apply the peak seeking scheme, we first check that all three assumptions from Section II are satisfied.

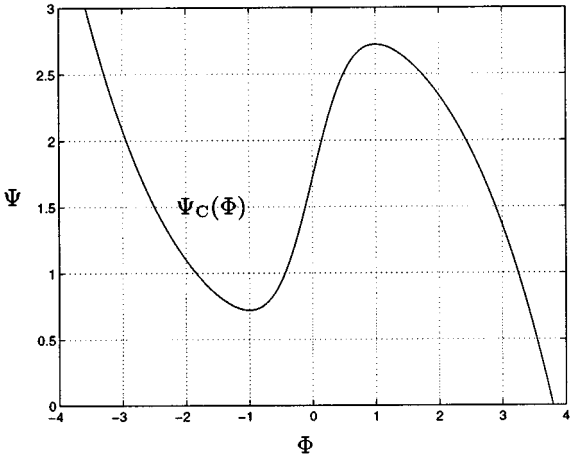

Fig. 2. Compressor characteristic $\Psi_C(\Phi)$.

1) From (3.4)–(3.7), Γ is given by

$$\Gamma = \Gamma_\Phi(\Phi_0) = 1 + \Phi_{C0} + \bar{\beta}^2(c_*\Phi_0 - c_\Psi \Psi_C(\Phi_0)) \tag{3.9}$$

where Φ_0 is the equilibrium value of Φ. In view of (3.8), it is clear that the function $\Gamma_\Phi(\cdot)$ is invertible. Thus, for each value of Γ, there is only one equilibrium $(\Phi, \Psi) = (\Gamma_\Phi^{-1}(\Gamma), \Psi_C(\Gamma_\Phi^{-1}(\Gamma)))$, which means that Assumption 2.1 is satisfied.
2) As we indicated above, it was proved in [14] that (3.8) guarantees that the equilibrium is exponentially stable not only locally but also globally, hence Assumption 2.2 is satisfied.
3) Following the notation in Section II, $y = h \circ l(\Gamma) \triangleq \Psi_C(\Gamma_\Phi^{-1}(\Gamma))$. The Moore–Greitzer model (3.1)–(3.3) is scaled so that $\Psi_C(\Phi)$ always has a maximum at $\Phi = 1$. Since $\Gamma_\Phi(\cdot)$ is bijective, $\Psi_C(\Gamma_\Phi^{-1}(\Gamma))$ has a maximum at

$$\Gamma^* = 1 + \Phi_{C0} + \bar{\beta}^2(c_* - c_\Psi \Psi_C(1)) \tag{3.10}$$

that is,

$$\left(\Psi_C \circ \Gamma_\Phi^{-1}\right)'(\Gamma^*) = 0 \tag{3.11}$$

$$\left(\Psi_C \circ \Gamma_\Phi^{-1}\right)''(\Gamma^*) < 0. \tag{3.12}$$

Hence, Assumption 2.3 is satisfied.

Since Assumptions 2.1–2.3 are satisfied, we can apply the peak seeking scheme given in Fig. 3 with

$$\Gamma = \hat{\Gamma} + a\sin\omega t. \tag{3.13}$$

By Theorem 2.1, for sufficiently small ω, δ, and $a, \Phi(t)$ converges to an $O(\omega + \delta + a)$-neighborhood of 1 and $\Psi(t)$ converges to an $O(\omega + \delta + a)$-neighborhood of its maximum value $\Psi_C(1)$.

The application of the peak seeking scheme to the surge model (3.5), (3.6) will make clearer the application to the full Moore–Greitzer model (3.1)–(3.3) in the next section.

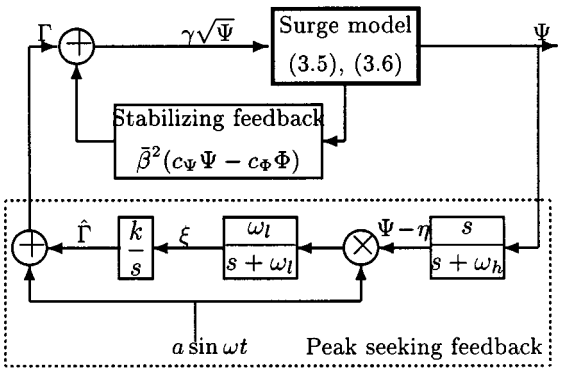

Fig. 3. Peak seeking scheme for the surge model (3.5), (3.6).

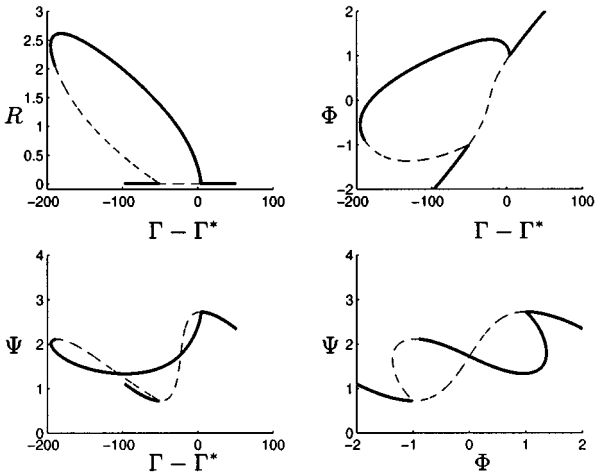

Fig. 4. Bifurcation diagrams for the case $\epsilon = 0.9, \beta = 1.42$, with the full-state controller. The control gains are $c_R = 30, c_\Psi = 7$ and $c_\Phi = 20$.

B. Peak Seeking for the Full Moore–Greitzer Model

Now we consider the full Moore–Greitzer model (3.1)–(3.3). In [15] we studied the stabilization of this model using the family of control laws

$$\gamma = \frac{\Gamma + \bar{\beta}^2(c_\Psi\Psi - c_\Phi\Phi + c_R R - d_\Phi\dot{\Phi})}{\sqrt{\Psi}} \tag{3.14}$$

and gave conditions for selecting the parameters c_Ψ, c_Φ, c_R, and d_Φ, such that local stabilization near the peak of the compressor characteristic is achieved. Fig. 4 shows bifurcation diagrams with respect to the parameter Γ, for the control law (3.14) with $d_\Phi = 0$, applied to the MG model with the compressor characteristic

$$\Psi_C(\Phi) = \Psi_{C0} + 1 + (1-\epsilon)\left(\frac{3}{2}\Phi - \frac{1}{2}\Phi^3\right) + \epsilon\frac{2\Phi}{1+\Phi^2}. \tag{3.15}$$

Treating (R, Φ, Ψ) as the state x, the equilibrium map $x = l(\Gamma)$ is given by the bifurcation diagrams in Fig. 4. The solid curves represent stabilized equilibria, while the dashed ones represent unstable equilibria. Like in Section III-A, we take $y = \Psi$ as the output that we want to maximize using the peak seeking scheme. Unfortunately, none of the three assumptions in Section II is satisfied: 1) the function $x = l(\Gamma)$ is multivalued; 2) the equilibrium at the peak is asymptotically stable but not exponentially stable; and 3) the output equilibrium map $y = h \circ l(\Gamma)$ has a maximum but it is not necessarily continuously differentiable. In spite of violating the assumptions, the peak seeking scheme can be applied to the full MG model. The scheme is given in Fig. 5. The closed-loop system is

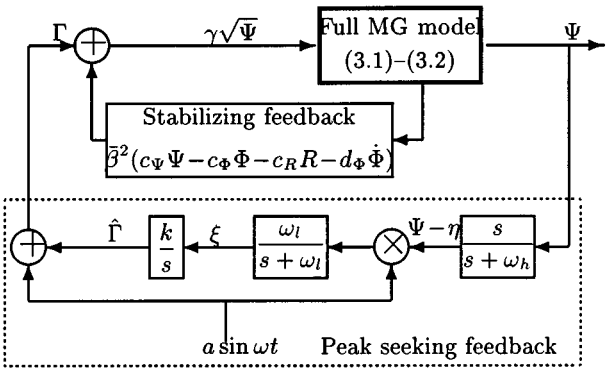

Fig. 5. Peak seeking scheme for the full Moore–Greitzer model (3.1)–(3.3).

$$\dot{R} = \frac{\sigma}{3\pi}\sqrt{R}\int_0^{2\pi}\Psi_C(\Phi + 2\sqrt{R}\sin\lambda)\sin\lambda\, d\lambda, \qquad R(0) \geq 0 \tag{3.16}$$

$$\dot{\Phi} = -\Psi + \frac{1}{2\pi}\int_0^{2\pi}\Psi_C(\Phi + 2\sqrt{R}\sin\lambda)\, d\lambda \tag{3.17}$$

$$\dot{\Psi} = \frac{1}{\beta^2}[1 + \Phi_{C0} - \hat{\Gamma} - a\sin\omega t - \bar{\beta}^2(c_\Psi\Psi - c_\Phi\Phi + c_R R - d_\Phi\dot{\Phi})] \tag{3.18}$$

$$\dot{\hat{\Gamma}} = k\xi \tag{3.19}$$

$$\dot{\xi} = -\omega_l\xi + \omega_l(\Psi - \eta)a\sin\omega t \tag{3.20}$$

$$\dot{\eta} = -\omega_h\eta + \omega_h y. \tag{3.21}$$

The multiple equilibria in the full MG model make the closed-loop system (3.16)–(3.21) considerably more difficult to analyze than the closed-loop system in the case of the surge model. The *solid* curve in the Ψ vs. $\Gamma - \Gamma^*$ plot in Fig. 4 plays the role of the function $\nu(\cdot)$ in the averaging analysis. Even though ν is not continuously differentiable, we can show that the average equilibrium is $O(a)$-close to the point $(R, \Phi, \Psi) = (0, 1, \Psi_C(1))$, that it is to the right of the peak (on the flat side of the solid curve on the Ψ vs. $\Gamma - \Gamma^*$ plot), and that it is exponentially stable. The singular perturbation analysis consists of a study of the reduced model and the boundary layer model. The averaging analysis establishes the existence of an exponentially stable $O(\omega + a)$-small periodic orbit of the reduced model—a conclusion no different than for

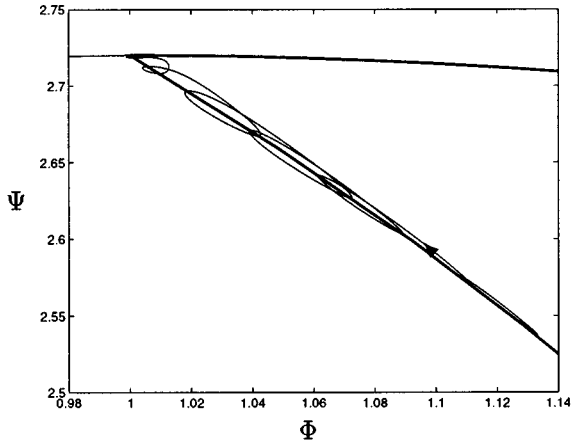

Fig. 6. A trajectory under the peak seeking feedback for $\omega = 0.03$ and $k = 0.4$.

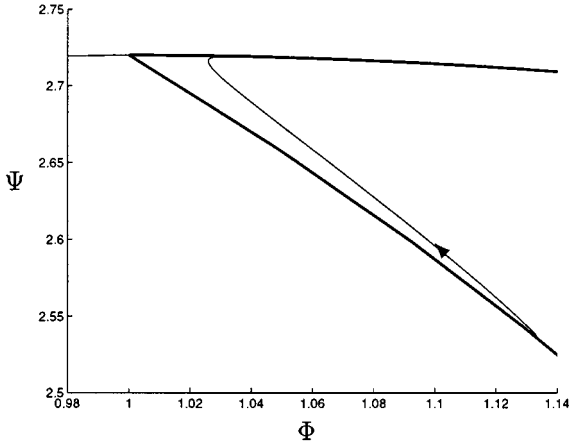

Fig. 7. A trajectory under the peak seeking feedback for $\omega = 0.03$ and $k = 1.5$.

the surge model. The difference comes in the analysis of the boundary layer model

$$\frac{dR_b}{dt} = \frac{\sigma}{3\pi}\sqrt{R_b}\int_0^{2\pi} \Psi_C(\Phi_b + 2\sqrt{R_b}\sin\lambda)\sin\lambda\, d\lambda \qquad R(0) \geq 0 \quad (3.22)$$

$$\frac{d\Phi_b}{dt} = -\Psi_b + \frac{1}{2\pi}\int_0^{2\pi} \Psi_C(\Phi_b + 2\sqrt{R_b}\sin\lambda)\, d\lambda \quad (3.23)$$

$$\frac{d\Psi_b}{dt} = \frac{1}{\beta^2}\left[1 + \Phi_{C0} - \Gamma - a\sin\omega t - \bar{\beta}^2\left(c_\Psi\Psi_b - c_\Phi\Phi_b + c_R R_b - d_\Phi\frac{d\Phi_b}{dt}\right)\right]. \quad (3.24)$$

Except for the equilibrium for $\Gamma = \Gamma^*$, the equilibria of interest in the boundary layer model are *exponentially* stable. The equilibrium for $\Gamma = \Gamma^*$ is only *asymptotically* stable. However any ball (with arbitrarily small but nonzero radius) around this equilibrium is exponentially stable. Or, to put it differently, the equilibrium for $\Gamma = \Gamma^*$ is exponentially *practically* stable with an arbitrarily small residual set. This set can be selected to be $O(\omega + a + \delta)$-small. Then by invoking Tikhonov's theorem on the infinite interval, we can draw the same conclusions as in Theorem 2.1, namely, that, for sufficiently small ω, δ, and a, the solution $(R(t), \Phi(t), \Psi(t), \hat{\Gamma}(t), \xi(t), \eta(t))$ converges to an $O(\omega + a + \delta)$-neighborhood of the point $(0, 1, \Psi_C(1), \Gamma^*, 0, \Psi_C(1))$.

C. Simulations for the Full MG Model

We now present simulations of the peak seeking scheme from Fig. 5 for a compressor with $\Phi_{C0} = 0, \Psi_{C0} = 0.72, \beta = 1.42, \epsilon = 0.9, \sigma = 4$, and with a stabilizing controller whose parameters are $\bar{\beta} = 1.42, c_\Psi = 2, c_\Phi = 4, c_R = 7, d_\Phi = 0$.

Our first simulation employs a peak seeking scheme with $a = 0.05, \omega = 0.03, \omega_h = 0.03, \omega_l = 0.01$, and $k = 0.4$. The trajectory is shown in Fig. 6, where the darker curve represents the trajectory and the lighter lines represent the axisymmetric and stall characteristics. The trajectory starts from an equilibrium on the stall characteristic and converges to a small periodic orbit near the peak of the compressor characteristic. If the peak seeking parameters are selected differently, for example, if k increased to $k = 1.5$, the new shape of the trajectory is shown in Fig. 7. In this case the convergence is smoother and faster but the periodic orbit is farther from the peak. (Note, however, that, given more time, the periodic orbit would slowly approach the peak.) Even though faster adaptation throws the periodic orbit further to the right of the peak, the periodic orbit remains in the "flat" region of the compressor characteristic where variations in mass flow Φ result in only minor variations of the pressure rise Ψ.

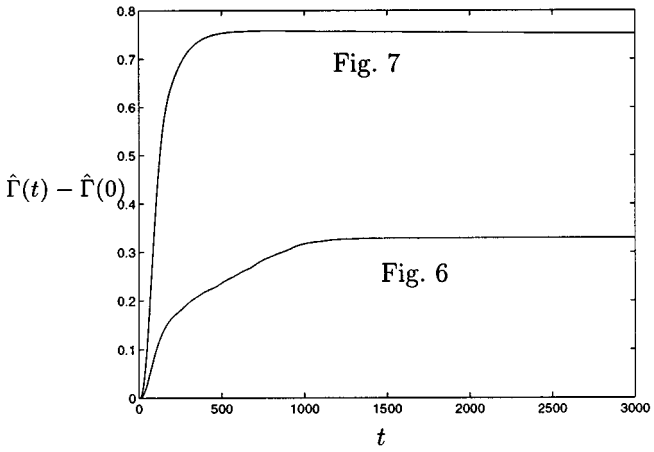

Fig. 8. Time response of $\hat{\Gamma}(t) - \hat{\Gamma}(0)$.

As explained in the previous section of the paper, the convergence of the trajectory to a close neighborhood of the peak is the result of regulating $\hat{\Gamma}(t)$ to a neighborhood of Γ^*. Fig. 8 shows the time traces of $\hat{\Gamma}(t) - \hat{\Gamma}(0)$ for the trajectories in Figs. 6 and 7. In this case $\hat{\Gamma}(0) = -1.2$ and $\Gamma^* = -0.90$, which means that $\Gamma^* - \hat{\Gamma}(0) = 0.30$. This explains why the trajectory in Fig. 6 converges closer to the peak than that in Fig. 7.

Since a permanent presence of the periodic perturbation is undesirable, we now show that it can be disconnected after a short peak seeking period. Fig. 9 shows the pressure transient

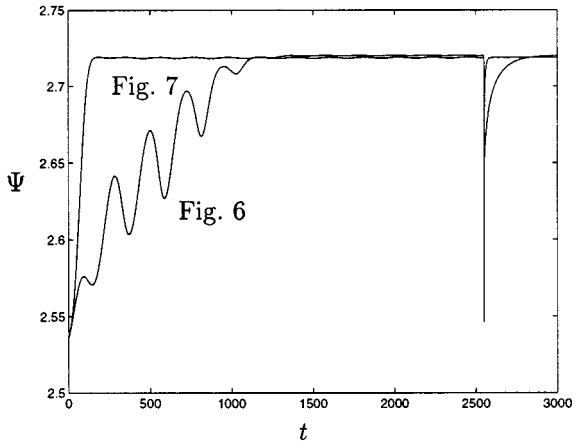

Fig. 9. Time response of the pressure rise. At $t = 2550$ we disconnect the peak seeking feedback.

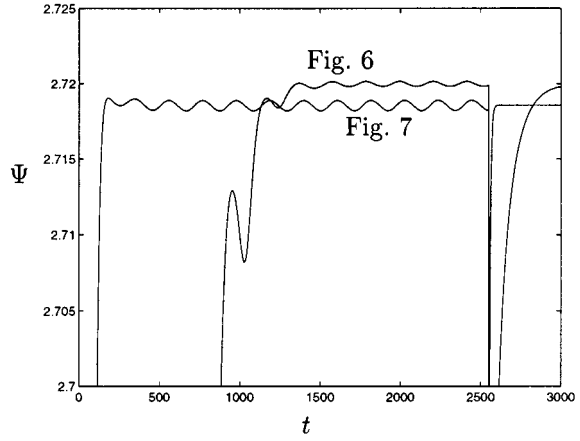

Fig. 10. Time response of the pressure rise on a scale where the variations are visible.

and steady state up to $t = 2550$, at which time, k and a are set to zero. The disconnection of adaptation makes the trajectory transition from the periodic orbit to an equilibrium on the compressor characteristic, just to the right of the peak. To make the transient more visible, we have set $R(2550+0) = 0.06$ because $R(2550-0)$ is practically zero. Fig. 9 also shows that the pressure variations in steady state under the peak seeking feedback are hardly noticeable, especially if compared to a large gain in the dc value of the pressure. To show the pressure variations more clearly, we zoom in on them in Fig. 10.

As mentioned above, while higher k speeds up adaptation, excessively high values of k are not helpful. For example, they can destabilize the desired equilibrium at the peak. Values of ω or a that are too high have been observed to have a similar effect. It would therefore be desirable to have bounds on k, ω, a, and the filter parameters used. Bounds derived from the singular perturbation and averaging analyses are useless because they are conservative and only conceptual. It is not clear how design bounds could be obtained analytically.

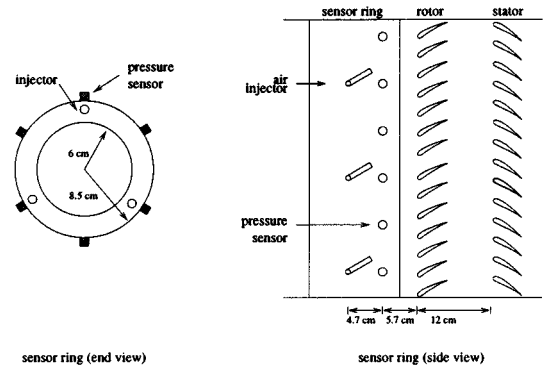

Fig. 11. Sensor and injection actuator ring.

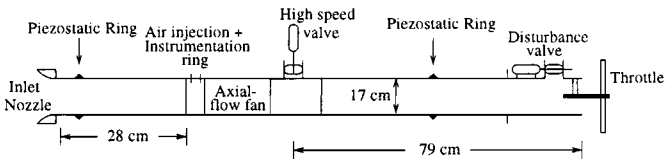

Fig. 12. Experimental setup.

IV. Experiment Results on Caltech Rig

A prerequisite for experimental validation of the scheme from Section III is the availability of a high-bandwidth bleed valve for stabilization of rotating stall. However, as shown in [4], rotating stall can also be stabilized by air injection. In this section we combine the air injection rotating stall controller from [4] with the extremum seeking scheme from Section II to achieve maximization of pressure rise.

A. Experimental Setup

Before we start, we point out that the experiment includes many effects not modeled in the theoretical part of the paper. For example, many dynamical phenomena in the real compressor are not captured by the MG3 model, and the filters used for processing of pressure measurements and elimination of noise introduce their own dynamic effects against which we provide no analytical guarantees. Nevertheless, as the experiments show, the peak seeking algorithms achieves the objective despite all these neglected effects.

Overall setup. The Caltech compressor rig is a single-stage, low-speed, axial compressor with sensing and actuation capabilities. Fig. 11 shows a magnified view of the sensor and injection actuator ring and Fig. 12 a drawing of the rig.

Compressor. The compressor is an Able Corporation model 29680 single-stage axial compressor with 14 blades, a tip radius of 8.5 cm, and a hub radius of 6 cm. The blade stagger angle varies from 30° at the tip to 51.6° at the hub, and the rotor to stator distance is approximately 12 cm. Experiments are run with a rotor frequency of 100 Hz, giving a tip Mach number of 0.17. Rotating stall is observed under this condition on the Caltech rig with a frequency of 65 Hz while surge occurs at approximately 1.7 Hz. Data taken for a stall transition event suggests

that the stall cell grows from the noise level to its fully developed size in approximately 30 ms (three rotor revolutions). At stall inception point, the velocity of the mean flow through the compressor is approximately 16 m/s.

Sensing. Six static pressure transducers with 1000-Hz bandwidth are evenly distributed along the annulus of the compressor at approximately 5.7 cm from the rotor face. A discrete Fourier transform is performed on the signals from the transducers, and the amplitude and phase of the first and second mode of the stall cell associated with the total-to-static pressure perturbation are obtained. The amplitude of the first mode is used for feedback. The difference between the pressure obtained from one static pressure transducer mounted at the piezostatic ring at the inlet and that from one mounted at another piezostatic ring downstream near the outlet of the system is computed as the pressure rise across the compressor. All of the static pressure transducer signals are filtered through a fourth-order Bessel low-pass filter with a cutoff frequency of 1000 Hz[1] before the signal processing phase in the software.

Air injection. The air injectors are on-off type injectors driven by solenoid valves. For applications on the Caltech compressor rig, the injectors are fed with a pressure source supplying air at a maximum pressure of 80 lbf/in^2. Due to significant losses across the solenoid valves and between the valves and the pressure source, the injector back pressure reading does not represent an accurate indication of the actual velocity of the injected air on the rotor face. For example, using a hotwire anemometer, the maximum velocity of the injected air measured at a distance equivalent to the rotor-injector distance for 50 and 60 lbf/in^2 injector back pressure are measured to be approximately 30.2 and 33.8 m/s, respectively. At the stall inception point, each injector can add approximately 1.7% mass, 2.4% momentum, and 1.3% energy to the system when turned on continuously at 60 lbf/in^2 injector back pressure. The bandwidth associated with the injectors is approximately 200 Hz at 50% duty cycle. Additional details on the air injection control are provided in [5], [29].

Peak seeking. Peak seeking is implemented via a bleed valve whose bandwidth is 51 Hz.

Computer. Implementation of all feedback laws (air injection and peak seeking) is performed digitally. The compression system hardware is interfaced with the real-time operating system software via a Pentium 100 MHz computer. A user-defined display interface is used to access the desired information.

B. Stall Stabilization

Stall stabilization is performed by air injection in a one-dimensional on-off fashion. When the measured amplitude of the first mode of the stall cell is above a certain threshold, all three injectors are fully open. Otherwise they are closed. The set point of the compressor is varied by a bleed valve. The characteristic of the pressure rise Ψ with respect to the bleed angle b is shown in the Fig. 13. The characteristic is obtained as follows: for each data point the system is first allowed 500 rotor revolutions over which to settle; the pressure and flow signals are then temporally averaged for 500 rotor revolutions to obtain the data point. Note that higher bleed angle means lower overall throttle opening. There is a clear peak in the characteristic curve. The points to the left of the peak are axisymmetric equilibria. The points to the right of the peak are stabilized low amplitude stall equilibria.

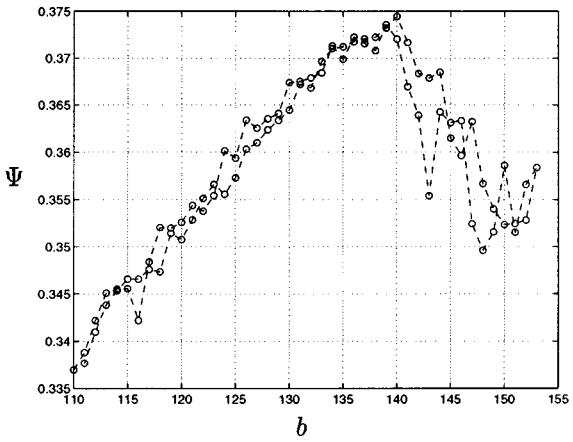

Fig. 13. Ψ versus bleed angle b.

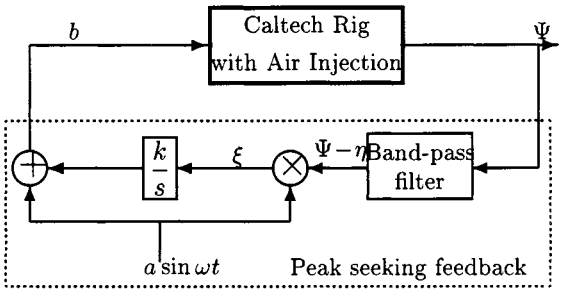

Fig. 14. Peak seeking scheme for the Caltech rig.

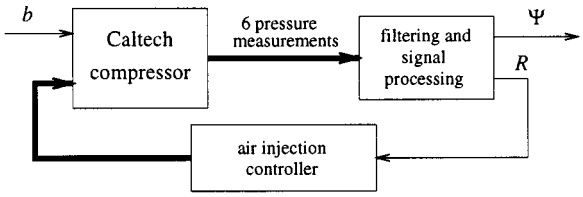

Fig. 15. Zooming in on the block "Caltech rig with air injection" in Fig. 14.

C. Filter Design

We implement the extremum seeking scheme in a configuration shown in Fig. 14. In the theoretical analysis in [16] noise was not considered and a high-pass filter $s/(s+\omega_h)$ was employed. Because of noise in the experiment we use a band-pass filter. From the power spectrum analysis, we learn that the noise is above 150 Hz. Also we know that the stall frequency is about 65 Hz. Since the filter should cut out both the high frequency noise and the stall oscillations, as well as dc, we choose the pass band to be 4 to 6 Hz, and implement it as third-order Butterworth filter. The perturbation signal used has a frequency of

[1]The first mode stall frequency is at approximately 65 Hz. The filter cutoff frequency is chosen to be 1000 Hz so that detection of higer modes can be carried out if desired. Also, the air injectors have a bandwidth of approximately 200 Hz. For the application of the extremum seeking algorithm, the use of a lower cutoff frequency will not affect the result significantly, unless the cutoff is sufficiently low to disrupt stall mode detection.

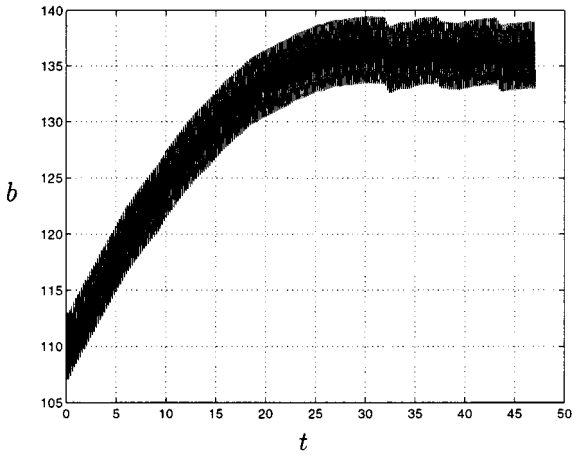

Fig. 16. The time response of the bleed angle initiating from the *axisymmetric* characteristic.

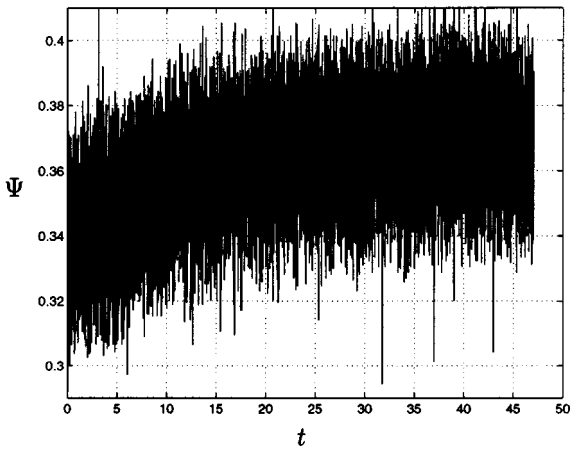

Fig. 17. The time response of the pressure rise initiating from the *axisymmetric* characteristic.

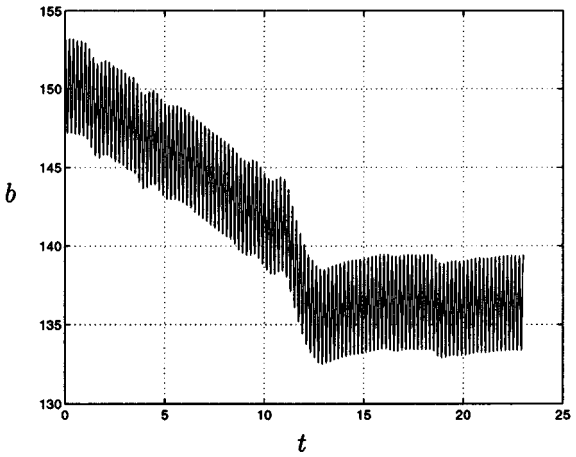

Fig. 18. The time response of the bleed angle initiating from the *stall* characteristic.

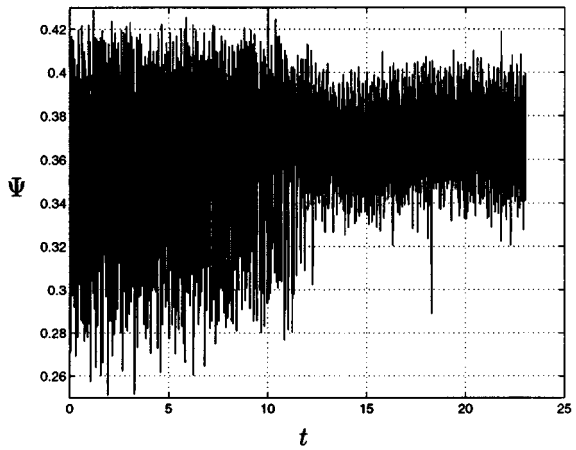

Fig. 19. The time response of the pressure rise initiating from the *stall* characteristic.

His research interests include nonlinear, adaptive, robust, and stochastic control theory for finite dimensional and distributed parameter systems, and applications to propulsion systems and flows 5 Hz, which is within the pass band. Theoretical considerations would dictate spacing the frequency of the perturbation (5 Hz) and the upper limit of the pass band of the filter (6 Hz) by an order of magnitude, to satisfy the conditions of the signular perturbation theorem. In this application, the small spacing of 1 Hz turns out to be sufficient. We do not use a low-pass filter $\omega_l/(s+\omega_l)$.

D. Experimental Results

1) Initial Point at Axisymmetric Characteristic: We select the integrator gain as 600 and set the frequency of the perturbation to 5 Hz. From Fig. 13 we know that the peak is around 134–139°. We set the initial bleed angle at 110°, the farthest point to the left in Fig. 13, and set the perturbation to 3°. The perturbed bleed angle is shown in Fig. 16 and the pressure rise response is shown in Fig. 17. Comparing the peak pressure rise 0.372 of Fig. 13 to that of Fig. 17, we see that they are the same.

2) Initial Point at Nonaxisymmetric Characteristic: For the compressor control, the most important issue is to control the system to avoid the stall that causes the deep pressure drop. Since the air injection can control stall for a reasonable interval, we can set the initial point at the stall characteristic. We select the initial point as 150° bleed valve angle because from Fig. 13 we can see that 150° is the largest angle we can achieve without a deep drop of the pressure rise. In this case we choose the gain of the integrator as 400. The perturbation signal is set to 3° as in the axisymmetric case. The perturbed bleed angle is shown in Fig. 18 and the pressure rise response is shown in Fig. 19. The peak pressure in Fig. 19 coincides with that in Fig. 13.

A closer look at Figs. 18 and 19 shows that the rotating stall amplitude reduces as the bleed angle reduces.

The effect of peak seeking on a system starting in rotating stall is to bring it out of stall without pushing the operating point away from the peak and reducing the pressure rise.

In both Figs. 16 and 18 one can observe fluctuations of the mean of the bleed angle at the peak. Comparing with Figs. 17 and 19, we see that these fluctuations occur at the same time when pressure drops resembling stall inception occur. Peak seeking reacts to this by pushing the operating point further to the right on the axisymmetric characteristic and then slowly returning it to the peak.

V. Conclusion

This experiment clearly shows that the concept of extremum seeking holds considerable promise for optimizing operation of aeroengines via feedback. The actuation requirements are much more modest than for stabilization of rotating stall and surge because the periodic perturbation applied for extremum seeking is slow compared to the compressor dynamics, and the sharp peak of the $\Psi(\Gamma)$ map allows the use of a perturbation signal of a very small amplitude so magnitude saturation does not become an issue. The sensing requirement is also modest because only the pressure rise Ψ is needed.

The extremum seeking has performed well in the high-noise experimental environment. In fact, the high noise makes the effect of the periodic perturbation hardly noticeable. The tuning of the control parameters was easy which speaks in favor of the extremum seeking scheme.

During the review of the paper a suggestion was made to provide a comparison—or explain why one is not possible—with a proportional integral derivative (PID) controller. This question helps reiterate the main point of extremum seeking control. As evident from any of the peak seeking diagrams in this paper, the scheme provides linear but *time-varying* feedback. It is due to the time-varying character that this feedback achieves regulation to an unknown equilibrium (an equilibrium which as a maximizer of the unknown equilibrium map). The PID or any other linear time invariant (LTI) controller would fail to achieve this objective.

References

[1] K. J. Astrom and B. Wittenmark, *Adaptive Control*, 2nd ed. Reading, MA: Addison-Wesley, 1995.

[2] A. Banaszuk and A. J. Krener, "Design of controllers for MG3 compressor models with general characteristics using graph backstepping," *Automatica*, vol. 35, pp. 1343–1368, 1999.

[3] R. L. Behnken, R. D'Andrea, and R. M. Murray, "Control of rotating stall in a low-speed axial flow compressor using pulsed air injection: Modeling, simulations, and experimental validation," in *Proc. 34th IEEE Conf. Decision Contr.*, 1995, pp. 3056–3061.

[4] R. D'Andrea, R. L. Behnken, and R. M. Murray, "Active control of rotating stall using pulsed air injection: A parametric study on a low-speed, sxial slow compressor," in *Proc. SPIE*, vol. 2494, Orlando, Florida, 1995, pp. 152–165.

[5] R. L. Behnken, "Nonlinear Control and Modeling of Rotating Stall in an Axial Flow Compressor," Ph.D. dissertation, California Inst. Technol., Pasadena, 1996.

[6] P. F. Blackman, "Extremum-seeking regulators," in *An Exposition of Adaptive Control*, J. H. Westcott, Ed. New York: Macmillan, 1962.

[7] C. S. Drapper and Y. T. Li, "Principles of optimalizing control systems and an application to the internal combustion engine," *ASME*, vol. 160, pp. 1–16, 1951. Also in R. Oldenburger, Ed., *Optimal and Self-Optimizing Control*, Boston, MA: MIT Press, 1966.

[8] K. M. Eveker, D. L. Gysling, C. N. Nett, and O. P. Sharma, "Integrated control of rotating stall and surge in aeroengines," presented at the 1995 SPIE Conference on Sensing, Actuation, and Control in Aeropropulsion, Orlando, FL, Apr. 1995.

[9] A. L. Frey, W. B. Deem, and R. J. Altpeter, "Stability and optimal gain in extremum-seeking adaptive control of a gas furnace," presented at the Proc. 3rd IFAC World Congr., 48A, London, 1966.

[10] E. M. Greitzer, "Surge and rotating stall in axial flow compressors—Part I: Theoretical compression system model," *J. Eng. Power*, pp. 190–198, 1976.

[11] G. Gu, A. Sparks, and S. Banda, Bifurcation-based nonlinear feedback control for rotating stall in axial compressors, vol. 68, pp. 1241–1257, 7.

[12] O. L. R. Jacobs and G. C. Shering, "Design of a single-input sinusoidal-perturbation extremum-control system," *Proc. Inst. Elect. Eng.*, vol. 115, pp. 212–217, 1968.

[13] V. V. Kazakevich, "Extremum control of objects with inertia and of unstable objects," *Sov. Phys. J.*, pp. 658–661, 1960.

[14] M. Krstić, D. Fontaine, P. V. Kokotović, and J. D. Paduano, "Useful nonlinearities and global bifurcation control of jet engine surge and stall," *IEEE Trans. Automat. Contr.*, vol. 43, pp. 1739–1745, 1998.

[15] M. Krstić and H. H. Wang, "Control of deep-hysteresis aeroengine compressors—Part II: Design of control laws," presented at the Proc. 1997 Amer. Contr. Conf., Albuquerque, NM.

[16] ——, "Design and stability analysis of extremum seeking feedback for general nonlinear systems," presented at the Proc. 1997 Conf. Decision Contr., TA02-3, San Diego, CA.

[17] M. Leblanc, "Sur l'electrification des chemins de fer au moyen de courants alternatifs de frequence elevee," *Rev. Gen. Elect.*, 1922.

[18] D. C. Liaw and E. H. Abed, "Active control of compressor stall inception: A bifurcation-theoretic approach," Automatica, vol. 32, pp. 109–115, 1996. Also in *Proc. IFAC Nonlinear Contr. Syst. Design Symp.*, Bordeaux, France, June 1992.

[19] F. E. McCaughan, "Bifurcation analysis of axial flow compressor stability," *SIAM J. Appl. Math.*, vol. 20, pp. 1232–1253, 1990.

[20] F. K. Moore and E. M. Greitzer, "A theory of post-stall transients in axial compression systems—Part I: Development of equations," *J. Eng. Gas Turbines Power*, vol. 108, pp. 68–76, 1986.

[21] I. S. Morosanov, "Method of extremum control," *Automat. Remote Contr.*, vol. 18, pp. 1077–1092, 1957.

[22] I. I. Ostrovskii, "Extremum regulation," *Automat. Remote Contr.*, vol. 18, pp. 900–907, 1957.

[23] J. D. Paduano, L. Valavani, A. H. Epstein, E. M. Greitzer, and G. R. Guenette, "Modeling for control of rotating stall," *Automatica*, vol. 30, pp. 1357–1373, 1966.

[24] A. A. Pervozvanskii, "Continuous extremum control system in the presence of random noise," *Automat. Remote Contr.*, vol. 21, pp. 673–677, 1960.

[25] R. Sepulchre and P. V. Kokotović, "Shape signifiers for control of surge and stall in jet engines," *IEEE Trans. Automat. Contr.*, vol. 43, pp. 1643–1648, 1998.

[26] J. Sternby, "Extremum control systems: An area for adaptive control?," in *Joint Amer. Contr. Conf.*, WA2-A, San Francisco, CA, 1980.

[27] G. Vasu, "Experiments with optimizing controls applied to rapid control of engine pressures with high amplitude noise signals," *Trans. ASME*, pp. 481–488, 1957.

[28] H. H. Wang, M. Krstić, and M. Larsen, "Control of deep-hysteresis aeroengine compressors—Part I: A Moore-Greitzer type model," presented at the Proc. 1997 Amer. Contr. Conf., Albuquerque, NM.

[29] C. Yeung, "Nonlinear Control of Rotating Stall and Surge with Axisymmetric Bleed and Air Injection on Axial Flow Compressors," Ph.D. dissertation, California Inst. Technol., Pasadena, 1998.

Hsin-Hsiung Wang received the B.Sc. and M.S. degrees in electrical engineering from Tatung Institute of Technology, Taiwan, and the M.S. and Ph.D. degrees in electrical engineering and mechanical engineering, respectively, from the University of Maryland, College Park, in 1996 and 1998, respectively.

Since 1998, he has been an Associate Professor at the Department of Electrical Engineering, Oriental Institute of Technology, Taiwan. His current research interests include bifurcation control and optimal performance seeking for aeroengine compressors, bioreactors, induction motors, and mass transport systems.

Chung-hei (Simon) Yeung is a native of Hong Kong. He received the B.S. degree in chemical engineering in 1993 from Case Western Reserve University, Cleveland, OH. He received the M.S. degree in 1996 and the Ph.D. degree in 1998, also in chemical engineering, from the California Institute of Technology, Pasadena.

He is currently with the Control Systems Program at General Electric, Corporate Research and Development.

Miroslav Krstić (S'92–M'95–SM'99) received the B.S.E.E. degree from the University of Belgrade, Yugoslavia, and the Ph.D. degree from the University of California, Santa Barbara, in 1994.

From 1995 to 1997 he was Assistant Professor of Mechanical Engineering at the University of Maryland. He is currently Associate Professor in the Department of Applied Mechanics and Egineering Sciences at the University of California, San Diego. His research interests include nonlinear, adaptive, robust, and stochastic control theory for finite dimensional and distributed parameter systems, and applications to propulsion systems and flows.

Dr. Krstić is a recipient of several paper awards, including the George S. Axelby Outstanding Paper Award of IEEE TRANSACTIONS ON AUTOMATIC CONTROL, and the O. Hugo Schuck Award for the best paper at American Control Conference. His doctoral dissertation received the UCSB Best Dissertation Award. He has also received the National Science Foundation Career Award, Office of Naval Research Young Investigator Award, and is the first recipient of the Presidential Early Career Award for Scientists and Engineers (PECASE) in the area of control theory. He is a coauthor of the books *Nonlinear and Adaptive Control Design* (New York: Wiley, 1995) and *Stabilization of Nonlinear Uncertain Systems* (New York: Springer-Verlag, 1998). He serves as Associate Editor for the IEEE TRANSACTIONS ON AUTOMATIC CONTROL, *International Journal of Adaptive Control and Signal Processing*, and *Systems and Control Letters*.